PREDICTION OF HEAT ACCUMULATION OF SYMMETRICAL RUBBER BUFFER ON TRACK-TYPE BULLDOZER

Jun Wang [1*] – Dagang Sun[1] – Shizhong Liu[2] – Yong Song[1] – Bijuan Yan[1] – Bao Sun[1]

[1] School of Mechanical Engineering, Taiyuan University of Science and Technology, Taiyuan, Shanxi, China
[2] School of Transportation and Logistics, Taiyuan University of Science and Technology, Taiyuan, Shanxi, China

ARTICLE INFO

***Article history*:**
Received: 16.9.2015.
Received in revised form: 20.2.2016.
Accepted: 24.2.2016.

Keywords:
Track-type bulldozer
Symmetrical rubber buffer
Heat accumulation
Hysteresis heat
Superficial temperature measurement

Abstract:

Symmetrical rubber buffers mounted on a track-type bulldozer are used in passive damping for the reduction of vibrations. As heat accumulation due to hysteresis may occur in continuous operation distributions of three typical cases were evaluated by FEM. The simulation result shows that hysteresis–related heat accumulation occurring near the contact region of the rubber pad remains unchanged in different cases. The maximum temperature in the case of earthmoving somewhat exceeds the range. The value of cutting and bulldozing is below the range. The value of loosening obviously exceeds the range. The great conductivity gap of heat flux between steel and rubber, which caused the most heat, was dissipated through the steel plate. Superficial temperatures were measured with a non-contact thermometer for the convenience of calculation that revealed a fair agreement between simulation and measurement in the case of earthmoving and cutting andbulldozing case. A lot of hysteresis-related heat produced due to excessive load caused a large error.

1 Introduction

The track-type bulldozer is one of the main forms of construction equipment for earthwork. Much vibration may be produced when the equipment operates off-road. Employing a symmetrical rubber buffer on the suspension of the equipment in passive damping may reduce noise and vibration efficiently [1], Fig. 1. The buffer consists of a steel plate and a natural rubber (NR) buffer. The hysteresis loss of the rubber, caused by the inherent phase difference between stress and strain, dissipates as heat due to the internal friction of the molecules. However, hysteresis heat may easily cause a temperature rise because of the poor thermal conductivity of the filled rubber. Mechanical properties will decrease in a hot environment, while high temperature may accelerate oxidation and fatigue, decreasing thereby the service life of the product [2].

Hysteresis heat of the rubber has been researched for several decades because it is difficult to determine the damping loss energy. The non-linearity of the material and deformation also cause difficulty in manual computation. Numerical methods are widely used for their effectiveness and convenience. Samuel et al. calculated the internal temperature distribution in an aircraft using a finite different method, linking the thermal and elastic characteristics with an empirical expression [3]. Whicker et al. presented a general concept to the analysis of the tire-steady

[*] Corresponding author. Tel.: +8603516998115
E-mail address: wj3201239@163.com

temperature. Three parts were determined: the structural module, dissipation module, and thermal module. The coupled thermo-mechanical problem was solved in an iterative manner with the finite element method (FEM) [4]. Allen et al. considered that energy dissipation from a cyclic inelastic deformation is the main heat generation source, and they made a transient conduction analysis [5]. Ebbott et al. predicted the tire rolling resistance and temperature distribution with FEM, especially considering the material properties and constitutive modeling [6]. Lin et al. investigated the temperature distribution in a smooth tread bias tire of a light truck with an uncoupled numerical procedure, operating under different speeds, pneumatic pressure, and loading condition [7]. Golbakhshi [8] and Tian et al. [9] used the same method to analyze the temperature distribution of a rolling tire. L. Pesek et al. used FEMLAB to solve the feedback thermo-mechanical interaction in a pre-pressed rubber block mounted on a resilient tram wheel [10]. Cho et al. predicted the temperature of a 3D tire with FEM, using a rational 4-parameter fit to interpolate the temperature dependence of the loss modulus of rubber [11]. Ghoreishy presented a review of the energy loss (rolling resistance) and temperature prediction [12]. Comparing the aforementioned references, the uncoupled solution is extensively used for a slow increase of the steady-state analysis when rubber is in the rubber-state, since it proved to be time and economic saving [13].

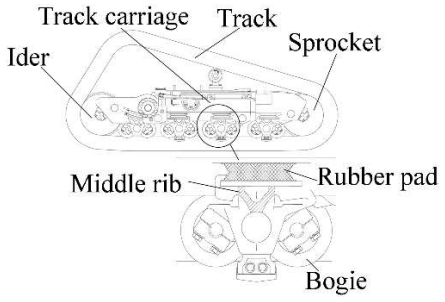

Figure 1. Assembly of the symmetrical rubber buffer

In this paper, heat accumulation of the symmetrical rubber buffer was evaluated using FEM. The tensile test of the rubber material was conducted in order to fit the Mooney-Rivlin constants. The hysteresis coefficient was obtained with the dynamic mechanical analysis (DMA). Steady-state temperature distributions of the buffer under typical cases were solved based on the uncoupled approach. The maximum values and position were found using the FEM simulation. Superficial temperatures were measured with a non-contact thermometer to verify the simulation. The block diagram is shown in Fig. 2.

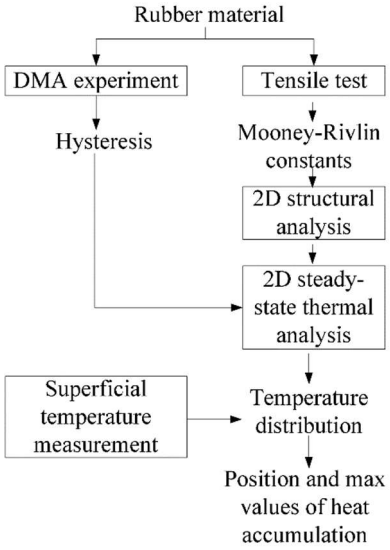

Figure 2. Block diagram of heat accumulation prediction

2 Material testing

2.1 Tensile testing of rubber material

One of the important characteristics of rubber–like materials is that they show a high degree of deformability under an action of comparatively small stresses. The force-extension is non-linear; hence mechanical behavior of these materials cannot be described as Hooke's law; instead, it is expressed in terms of the strain energy potential [14]. These materials are termed hyperelastic. The hyperelastic constitutive relation has a sophisticated nonlinear solution in the FEM software. There are several constitutive models described as the mechanical behavior of rubber. One group of models is based on the physically-motivated model, such as the Arruda-Boyce model and the Van der Waals model. The other is based on the phenomenological model, such as the polynomial (order *N*), including the Mooney-Rivlin model, the Reduced polynomial (Neo-Hookean & Yeoh) model, the Ogden model, and the Marlow model [15]. The Mooney-Rivlin model is suitable to describe middle and small strain, expressed as

$$U = \mathrm{C}_{10}(I_1 - 3) + \mathrm{C}_{01}(I_2 - 3) \qquad (1)$$

where U is the strain energy density (J·m^{-3});

C_{10} and C_{01} are the Mooney-Rivlin constants (Pa);

I_i are the deviatoric strain invariants, which are defined as

$I_1 = \lambda_1^2 + \lambda_2^2 + \lambda_3^2$ and $I_2 = \lambda_1^2\lambda_2^2 + \lambda_2^2\lambda_3^2 + \lambda_3^2\lambda_1^2$

where λ_i are the principal stretches,

$\lambda_1\lambda_2\lambda_3 = 1$.

For a uniaxial extension and again for simplicity, the nonlinear stress-strain relationship of a Mooney-Rivlin type material was expressed as

$$\sigma = 2\left(\lambda - \frac{1}{\lambda^2}\right)\left(C_{10} + \frac{C_{01}}{\lambda}\right) \quad (2)$$

where σ is the stress;

$\lambda = \varepsilon + 1$ is the expansion ratio;

ε is the strain.

The uniaxial tension of the dog bone sample was carried out on a MTS 350-10kN material testing machine (Testometric, UK), according to ISO37:2005. A stable agreement was present between the fitting curve and test data. The Mooney-Rivlin constants C_{10} and C_{01} were obtained via fitting testing data of stress versus strain (Fig. 3).

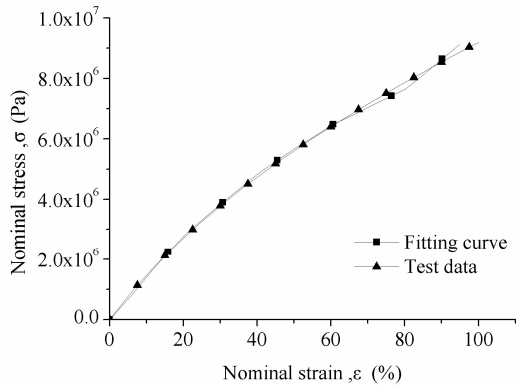

Figure 3. Comparison between the fitting curve and test data

2.2 Hysteresis testing of rubber material

The phase between the storage modulus E' and the loss modulus E'' represents hysteresis in solid rubbers, complex modulus E^* can be expressed as:

$$E^* = \sqrt{(E')^2 + (E'')^2} \quad (3)$$

$$H = \frac{E''}{E^*} \quad (4)$$

A 50 mm×10mm×2 mm strip was evaluated against a three-point bending test on DMA242c (NETZSCH, Germany). The warm-up speed is 4℃/min. E' and E^* varied with temperature and frequency, were obtained with the style of a multi-frequency synchronous scan [16,17]. The curves of hysteresis under different frequencies kept smooth and tended to be invariable and reached 0.15 (Fig. 4).

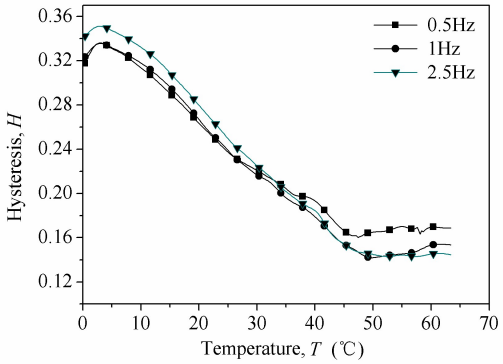

Figure 4. Hysteresis of different frequencies

3 Numerical simulation

3.1 FEM method

The analysis process was carried out using the commercial software ANSYS. The analysis was separated into the structural module and thermal module independently, linked with a dissipation computation. In the structural module, steel is identical to the linear elastic isotropic material, meshed with a Plane182 element; rubber is identical to a nonlinear hyper-elastic isotropic material; it is homogeneous and nearly incompressible, meshed with a Plane183 element. The mechanical characteristics and thermal conductivity of materials have no temperature dependence. The steel plate and rubber pad were mapped meshed. The penalty contact method and the Lagrange multiplier were used to solve the nonlinear contact problem. Nlgeom option should be ticked in the nonlinear solution.

The strain energy density (strain energy per unit of volume) is obtained through a structure analysis. Strain energy is the potential energy stored during elastic deformation. It is commonly used during the loading-unloading cycles [18]. The modal analysis of the modal damping ratios of the structure are

estimated from the undamped normal mode results by means of the modal strain energy method [19, 20], but damping loss energy cannot be obtained accurately just yet. Hysteresis H indicates the portion of the hysteresis loss energy in total energy. Equation (4) is also written as [7], [9]:

$$H = \frac{E^{"}}{E^{*}} = \frac{U_{\text{loss}}}{U_{\text{total}}} \tag{5}$$

Therefore heat generation H_g can be written as:

$$H_g = U_{loss} \cdot f = U_{total} \cdot H \cdot f \tag{6}$$

f represents vibration frequency.

In the thermal module, the structural element should be changed into the thermal element Plane55. With the help of a combined equation (6), with the result of the structural analysis, the heat generation H_g was computed and applied on each node as thermal load. Friction heat is negligible for the low sliding probability between the upper pad and lower pad.

3.3 Boundary condition

The upper steel plate of the buffer is fixed on the frame and the down steel plate is assembled with a bogie. Vibration may be transmitted to the buffer through the bogie. If the local coordinate is established on the frame of the equipment, then all degrees of freedom are fixed on the upper plate and vertical pressure P is applied on the down plate. The pressure and frequencies are different under three cases. The frequency is low in heavy load and vice versa.

The movement of the bulldozer off-road is random and lower, approximately 3~10km/h (1~3m/s). Considering that the experiment would be operated in indoor surroundings, the thermal convection between the buffer and outer space is assumed as a natural convection about the vertical cylinder in an infinite space, heat transfer coefficient between a fluid medium and the surface was obtained by experimental correlative formula:

$$N\mu_m = C(G_{\text{r}} \cdot P_{\text{r}})^n_{\text{m}} \tag{7}$$

where $N\mu_{\text{m}}$ is the Nusselt number of natural convection in an infinite space, subscript m means that qualitative temperature is arithmetic mean temperature difference T_{m}, $T_{\text{m}} = (T_{\text{a}} + T_{\text{s}})/2$;

T_{s} is the virtual superficial temperature for computing essential boundary conditions. For ideal gas, the expansion coefficient is equal to $\alpha_v = 1/T$ in G_r.

See the computational procedure in the reference [21];

Natural convection in an infinite space can be computed with the formula $h_f = Nu\frac{\lambda_{\text{c}}}{l}$. λ_{c} is thermal conductivity. The initial temperature distribution is uniform and equal to ambient temperature 20℃.

3.4 Conservation equation

Thermal energy is assumed to be completely converted with hysteresis heat generation. The temperature gradient along the circumferential direction is neglected. After a long-term loading, the temperature distribution of the buffer tends to be steady, therefore, it is regarded as a 2D steady heat transfer with internal heat source, expressed as [22]

$$J[T(x,y)] = \iint_D \left[\frac{k}{2}\left(\frac{\partial T}{\partial x}\right)^2 + \frac{k}{2}\left(\frac{\partial T}{\partial y}\right)^2 - q_v T\right]dxdy + \oint_\Gamma \alpha\left(\frac{1}{2}T^2 - T_f T\right)ds \tag{8}$$

where k is thermal conductivity;

q_v represents the rate of volumetric heat;

T_f is medium temperature;

α is the heat transfer coefficient between a fluid medium and the surface.

The 2D axi-symmetric finite element model is established as shown in Fig. 5.

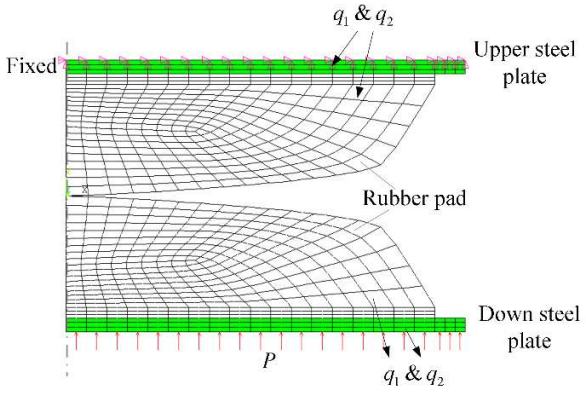

Figure 5. 2D axi-symmetric FE model

Material properties of steel and rubber are shown in Table 1.

Table 1 Material properties of steel and rubber

Properties	Material	
	Steel	Rubber
Density (kg/m^3)	7850	1130
Young's modulus (Pa)	$2.1 \cdot 10^{11}$	—
Poisson' ratio	0.3	0.499
Mooney-Rivlin constants (Pa)	—	$C_{10}=1.24 \cdot 10^6$ $C_{01}=0.025 \cdot 10^6$
Friction coefficient	—	0.5
Specific heat capacity (J/kgK)	502	1830
Thermal conductivity, (W/m℃)	70	0.25
Emissivity	0.2	0.95
Hysteresis	—	0.15

4 Result and Discussion

4.1 Simulation result

Steady-state temperature distributions of three typical cases were solved using FEM. The treads of temperature distributions were similar and each distribution was symmetrical.

Temperature distributions decreased gradually as concentric circles. Contour plots of temperature distributions are shown in Fig. 6 (a), Fig. 7 (a), and Fig. 8 (a). The positions of heat accumulation that remained unchanged are located in the contact regions between the upper and down rubber pad where hysteresis heat was produced. The temperature range of most natural rubber is -30 - 60℃. The maximum value of the earthmoving case is slightly out of the service range, in which case the frequency is higher but the load is lighter.

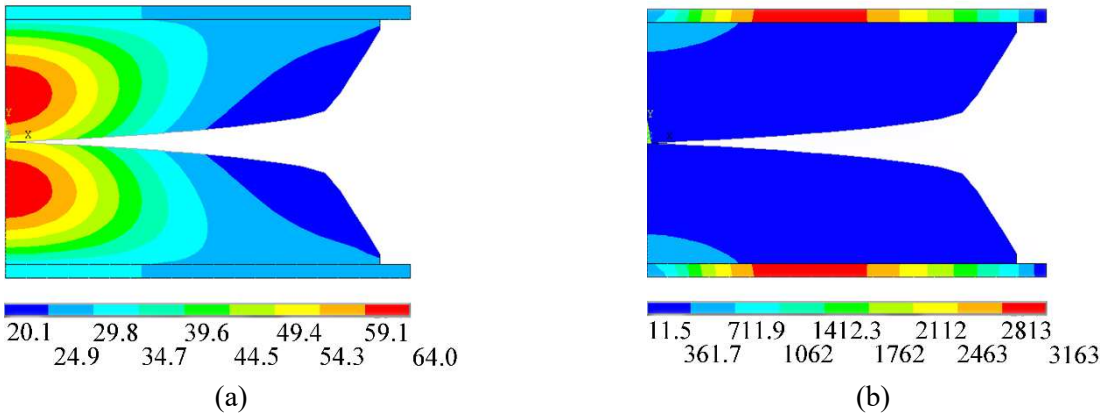

Figure 6. Contour plots of temperature distribution and the corresponding heat flux under earthmoving

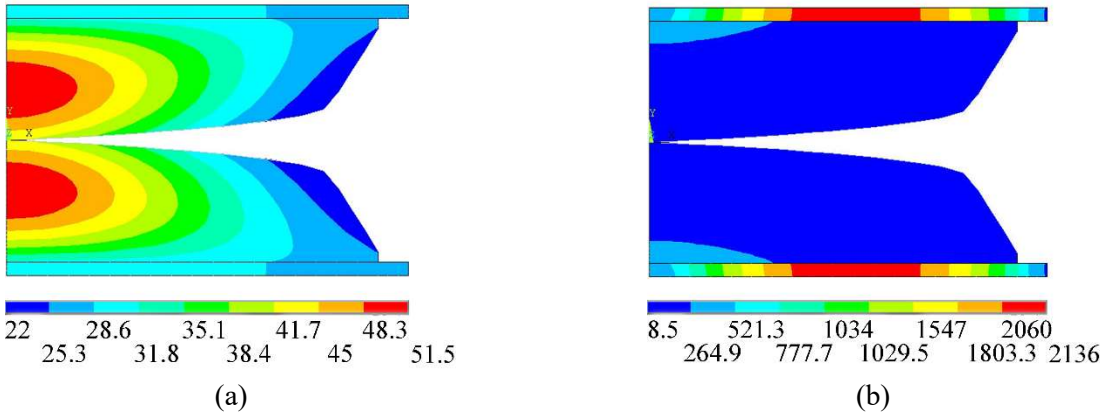

Figure 7. Contour plots of temperature distribution and the corresponding heat flux under cutting and bulldozing

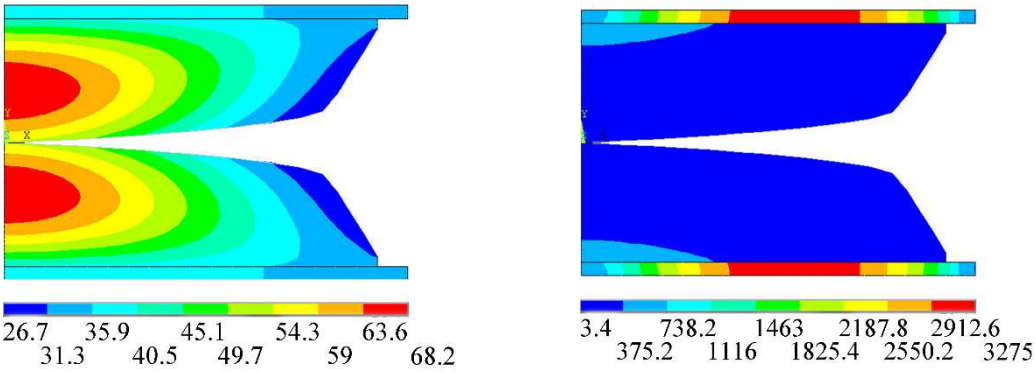

Figure 8. Contour plots of temperature distribution and the corresponding heat flux under loosening

The maximum value of the cutting and bulldozing case is obviously below range. The maximum value of the case of loosening that is apparently out of range can reach up to 68.2℃.

The heat flux of the steel plate is much bigger than that of the rubber pad. It shows that heat is almost dissipated from the steel plate due to a big gap of conductivity and specific heat capacity between both materials. Therefore the heat flux of rubber is nearly uniform and low. The heat flux of rubber-steel interfaces is somewhat lower than the values in the bulk rubber. Contour plots of the heat flux are shown in Fig. 6 (b), Fig. 7 (b), and Fig. 8 (b). The dimension of rubber may not be thicker in design so as to accelerate the heat diffusion.

4.2 FEM model validation

By contrast, superficial temperatures T_m of rubber pads were measured so as to verify the simulation result. Since it is complicated to measure the internal temperature directly, the compression test was performed indoors on an electro-hydraulic servo and program-controlled testing machine (Fig. 9). Ambient temperature was approximately 20. T_m was measured in some directions with the non-contact thermometer. A fair agreement was found between the simulated superficial temperature T_s and T_m under an earthmoving case and cutting and bulldozing case, quite similar to the ambient temperature. Emissivity, distance, air transparency, and production technology of materials may cause a slight error. A large error between T_s and T_m occurred under a loosening case. Thermal softening and minor cracks appeared in the process. Excessive hysteresis heat produced under heavy load caused a temperature increase. Load has a great influence on the temperature rise [23]. Time-dependent (viscoelasticity) [24] and damage effect [25] should be considered simultaneously. The contrast between simulation and measurement is shown in Table 2.

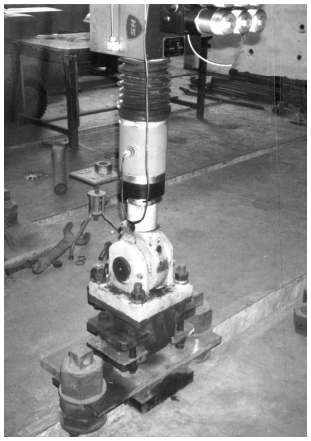

Figure 9. Compression test setup

Table 2. Superficial temperature contrasts between simulation and measurement

Cases	P/kN	f/Hz	T_s/℃	T_m/℃
Earthmoving	75	2.5	20.1	22.4
Cutting & bulldozing	150	1.0	22.0	20
Loosening	200	0.5	26.7	58.5

5 Conclusion

Heat accumulation caused by hysteresis of the symmetrical rubber buffer on a track-type bulldozer was evaluated with a FEM simulation. The stress-strain tensile test and hysteresis coefficient measurement were carried out for the simulation.

Hysteresis loss as an internal heat source was obtained from the structural analysis result. Steady-state thermal solutions under three typical cases (earthmoving, cutting and bulldozing, and loosening) were solved with boundary conditions. The tread of temperature distributions was similar and the heat accumulation position occurred in the contact region of the rubber pad invariably. Superficial temperatures were measured indoors with a non-contact thermometer. There is a fair agreement between simulation and measurement under an earthmoving case and cutting and bulldozing case. A large error occurred under a loosening case. Excessive hysteresis heat produced by a heavy load causes thermal softening and minor cracks. Load has a great influence on the temperature rise.

Acknowledgments

The work was funded by the National Natural Science Foundation for Young Scientists of China (Grant No.51405323), National Natural Science Foundation for Young Scientists of China (Grant No.51305288), Natural Science Foundation for Young Scientists of Shanxi province (Grant No.2013021020-1), and Postgraduate Outstanding Innovation Project of Postgraduate of Shanxi province (Grant No.2014-1).

References

[1] Sun D.G., Song Y., Lin M.Y., Zhang X.L.: *Modeling of dynamic contact finite element method for damping buffer components mounted on viscoelastic suspensions*, Transactions of the CSAE, 24 (2008), 1, 24-28.

[2] Ayoub G., Zaïri F., Naït-Abdelaziz M., Gloaguen J.M., Kridli G.: *A visco-hyperelastic damage model for cyclic stress-softening, hysteresis and permanent set in rubber using the network alteration theory*, International Journal of Plasticity, 54 (2014), 3, 19-33.

[3] Samuel K.C., Dodge R.N.: *Tire modeling and contact problems heat generation in aircraft tires*. Computers & Structures, 20 (1985), 1-3, 535-544.

[4] Whicker D., Browne A.L., Segalman D.J., Wickliffe L.E.: *A thermomechanical approach to tire power loss modeling*, Tire Science and Technology, 9 (1981), 1-4, 3-18.

[5] Allen J.M., Cuitino, A.M., Sernas V.: *Numerical investigation of the deformation characteristics and heat generation aircraft tires: Part . Thermal modeling*, Finite Elements in Analysis and Design, 23 (1996), 2, 265-290.

[6] Ebbott T.G., Hohman R.L., Jeusette J.P., Kerchman: *Tire temperature and rolling resistance prediction with finite element analysis*, Tire Science and Technology, 27 (1999), 1, 2-21.

[7] Lin Y.J., Hwang S.J.: *Temperature prediction of rolling tires by computer simulation,* Mathematics and Computers in Simulation, 67 (2004), 3,235-249.

[8] Golbakhshi H., Namjoo M., Mohammadi M.: *Evaluating the Effect of Dissipated Viscous Energy of a Rolling Tire on Stress, Strain and Deformation Fields Using an Efficient 2D FE Analysis*, International Journal of Automotive Engineering, 4 (2014), 1, 629-637.

[9] Tang T., Johnson D., Smith R.E., Felicelli S.D.: *Numerical evaluation of the temperature field of steady-state rolling tires*, Applied Mathematical Modeling, 38 (2014), 5-6, 1622-1637.

[10] Pešek L., Půst, L., Šulc, P.: *Thermo-mechanical properties of compressed rubber block*, Engineering Mechanics, 14 (2007), 1-2, 3-11.

[11] Cho J.R., Lee H.W., Jeong W.B.: *Numerical estimation of rolling resistance and temperature distribution of 3-D periodic patterned tire*, International Journal of Solids and Structures, 50 (2013), 1, 86-96.

[12] Ghoreishy M.H.R.: *A state of the art review of the finite element modeling of rolling tyres,* Iranian Polymer Journal, 17 (2008), 8, 571-597.

[13] Le Chenadec Y., Raoult I., Stolz C., Nguyen-Tajan T.M.L.: *Cyclic approximation of the heat equation in finite strains for the heat build-up problem of rubber*, Journal of Mechanics of Materials & Structures, 4 (2009), 2, 309-318.

[14] Zhuang Z., Zhang F., Qin S., et al. *ABAQUS nonlinear finite element analysis and living example*, Science Press, Beijing, 2005.

[15] Dassault, Inc. *Modeling rubber and viscoelasticity with ABAQUS*, 2009.

[16] Dee P.P., Choudhury, N.R., Dutta N.K.: *Thermal Analysis of Rubbers and Rubbery Materials*, iSmithers, London, 2010.

[17] Wagner M. Translated by Lu LM. : *Thermal analysis in practice*, Donghua University Press, Shanghai, 2011.

[18] Ghoreishy M.H.R.: *Finite element analysis of the steel-belted radial tire with tread pattern under contact Load*, Iranian Polymer Journal, 15 (2006), 8, 667-674.

[19] Johnson, C. D., Kienholz D. A.: *Finite Element Prediction of Damping in Structures with Constrained Viscoelastic Layers*. AIAA Journal, 20 (1982), 9, 1284-1290.
[20] Luo, J., Liu X. *An approximate response of the large system with local cubic nonlinearities subjected to harmonic excitation*. Engineering Review, 35 (2015), 1, 49-59.
[21] Yang S.M., Tao W.Q.: *Heat transfer (4th edition)*, Higher Education Press, Beijing 2006.
[22] Bergheau J.M., Fortunier R.: *Finite element simulation of heat transfer*, John Wiley & Sons, Inc., London, 2008.
[23] Li, Y., Zuo S. G., Duan X. L.: *Test analysis of temperature field distribution of tires and its influencing factors*. Journal of tongji university (Natural science), 40 (2012), 8, 1249-1253.
[24] Yang T.Q. *Viscoelastic theory and applications*, Science Press, Beijing, 2004.
[25] Shangguan W.B., Liu T.K., Wang X.L., Xu C., Yu B.: *A method for modeling of fatigue life for rubbers and rubber isolators*, Fatigue & Fracture of Engineering Materials & Structures, 37 (2014), 6, 623 – 636.